Journal of Power Sources 195 (2010) 6941–6944

Contents lists available at ScienceDirect

Journal of Power Sources

journal homepage: www.elsevier.com/locate/jpowsour

Short communication

Counter flow membraneless microfluidic fuel cell

Kamil S. Salloum[a], Jonathan D. Posner[a,b,*]

[a] Mechanical Engineering, Arizona State University, Tempe, AZ 85287, USA
[b] Chemical Engineering, Arizona State University, Tempe, AZ 85287, USA

ARTICLE INFO

Article history:
Received 2 March 2010
Received in revised form 30 March 2010
Accepted 30 March 2010
Available online 7 April 2010

Keywords:
Membraneless fuel cell
Porous electrodes
Vanadium flow battery
Microfluidic fuel cell

ABSTRACT

A counter flow membraneless microfluidic fuel cell is presented, where a non-reacting electrolyte separates the reacting streams. In this fuel cell design, vanadium reactants flow through porous carbon electrocatalysts. A sulfuric acid stream is introduced in the gap between the electrodes and diverts the reactants to opposite and independent outlets. This fuel cell differs from other membraneless designs in its ability to maintain a constant separation between the reactants without diffusive mixing.

1. Introduction

Small scale fuel cells have attracted considerable interest over the past several years for their potential use as power sources in portable electronic devices [1–3]. Miniaturization efforts have primarily aimed at scaling down common PEM fuel cell architectures [4], however such systems retain challenges found in their full scale counterparts, such as membrane degradation [5], water management [6], fuel crossover [7], and required humidification of the reactant streams [8]. More recently, microfluidic fuel cells have been developed that leverage laminar liquid flow of the reactants as a substitute for a solid polymer membrane [9–28]. Liquid electrolyte based reactants typically have greater energy densities and are safer to use, store, and handle [29]. Membraneless fuel cells suffer from higher Ohmic losses than membrane based systems due to the larger distances between the electrodes.

Most of the existing research on microfluidic membraneless fuel cells focus on the study and optimization of the co-flowing parallel streams of liquid fuel and oxidant [30]. In low Reynolds number regimes ($Re < 1$), co-flowing streams develop a laminar interface which serves as the ion exchange zone between the two electrodes of the fuel cell. The reactants are typically consumed along the entire length of the microchannel as they travel downstream. Higher flow rates result in higher power densities since the mass transport boundary layer is thinner at the electrode surfaces, resulting in higher reaction rates [14]. This power increase is at the expense of fuel utilization since higher flow rates advect reactants downstream before they can be consumed. Moreover, unreacted fuel and oxidant at the interface will mix by diffusion, resulting in depletion of the overall reactant availability, or mixed potential if either reactant reaches its counter-electrode. Membraneless fuel cells have been demonstrated with vanadium [2,21,22,24], formic acid [13,27], hydrogen saturated electrolytes [15,16,28], gaseous electrolytes [18,25], peroxide [19], and have been tested in both basic and acidic media [9,10,23].

In our previous work, we presented a membraneless fuel cell where the fuel and oxidant flow in series [27]. The sequential flow design eliminates the linear diffuse interface responsible for reactant mixing and crossover in parallel flow schemes. We also used porous electrodes to increase the overall reaction surface area that results in higher fuel utilization. In this serial design any unutilized fuel will either mix and deplete the oxidant, or react at the cathode and cause mixed potentials. Therefore the sequential flow pattern requires complete utilization of the reactant traveling through both electrodes, or pairing a fuel and oxidant with selective catalysts. Kjeang et al. presented a parallel flow scheme where the reactants also flow through porous electrodes prior to their diffusive interface [22]. The flow through design alleviates complications with the diffusion boundary layer growth on sidewall electrodes, which is typical in parallel flow architectures. In both studies, power density increased with increasing flow rate, countered by a decrease in fuel utilization. Moreover, stronger electrolytes increase the power density due to enhanced conductivity in the fuel cell.

In this work, we present a counter flow membraneless microfluidic fuel cell relying on vanadium redox species. The vanadium redox flow battery (VRB) uses the multiple oxidation states of vanadium as half-cells separated by an ion exchange membrane [31].

* Corresponding author at: Mechanical Engineering, Arizona State University, Tempe, AZ 85287, USA. Tel.: +1 480 965 1799; fax: +1 480 965 1384.
E-mail address: jposner@asu.edu (J.D. Posner).

0378-7753/$ – see front matter © 2010 Elsevier B.V. All rights reserved.
doi:10.1016/j.jpowsour.2010.03.096

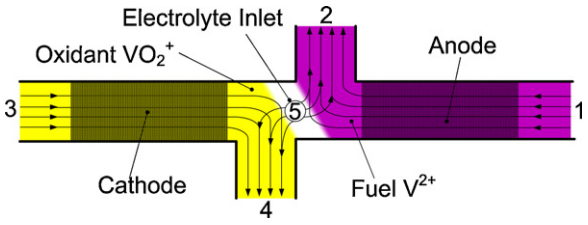

Fig. 1. Counter flow fuel cell schematic. The reactants are introduced at opposite ends (1,3) and flow through porous electrodes. An electrolyte is introduced at the interface of the reactants (5) which direct their flow to outlets (2,4) while completing the electrochemical circuit.

Here we use a non-reacting electrolyte to separate the reacting streams. Fig. 1 shows a schematic of the counter flow pattern with porous electrodes. The fuel is introduced from port 1, undergoes oxidation at its porous anode, and then exits the cell through port 2. The oxidant, in a similar manner, is introduced from port 3, undergoes reduction at its porous cathode, and then exits through port 4. The electrolyte serves as a non-reacting, ion conductive medium that is introduced at the center of the cell through port 5. The electrolyte prevents the direct interface between the fuel and oxidant. The electrolyte flow splits equally to exit through ports 2 and 4. The electrons are conducted externally from the anode to cathode through a characterization platform (not shown). Fig. 2 shows particle streak imaging of the counter flow scheme, with the electrolyte stream absent for simplifying the visualization. A video of the visualization is provided as Supplemental material to this manuscript.

The counter flow design provides several improvements to previous multi-stream designs. Sun et al. [28] presented a three stream membraneless fuel cell using the parallel flow scheme. While the design effectively separated the fuel and oxidant, the distance between the electrodes was increased – resulting in higher Ohmic losses – and a concentration boundary layer still developed over the sidewall electrodes, causing depletion zones for the reactants downstream. Jayashree et al. [18] and Brushett et al. [9,10] also presented microfluidic fuel cells with flowing electrolytes, however the separation was maintained with a solid porous diffusion layer rather than fluidics, thereby enlarging the fuel cell and adding complexity to its fabrication and construction. The counter flow design we present here prevents the reactants from mixing in two ways: (i) by using hydrodynamics to prevent diffusive mixing at the interface, and (ii) by independently collecting the reactants through separate outlets, allowing for a possible reuse.

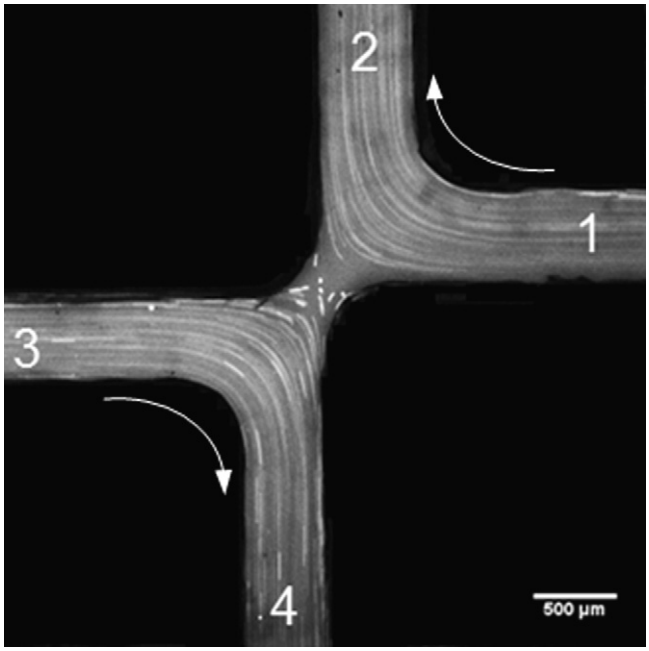

Fig. 2. Particle streaking flow visualization of a counter flow scheme. One stream flows from inlet 1 to outlet 2, while the other stream flows from inlet 3 to outlet 4. For simplicity in the imaging, these two streams are interacting without the source of an electrolyte in the center.

2. Experimental methods

In this section we present a brief overview of the experimental setup and conditions. An expanded description of the materials, construction, and preparation of the fuel cell and chemistry is provided as Supplemental information to this manuscript. The fuel cell housing and fluidic channels are constructed from laser ablated PMMA plastic. The channels' cross section is 1 mm^2 which embeds 10 mm long porous carbon (E-TEK, Somerset, NJ) electrodes which acts as the catalyst. The porous catalyst comes in contact with 10 mm long, 0.127 mm wide platinum wire for external electrical connections. The fuel cell receives reactants (50 mM vanadium species in 1 M sulfuric acid) and separation electrolyte (2 M sulfuric acid) through two separate syringe pumps. Reactant flow rates ranged from 50 to 2000 $\mu l\,min^{-1}$, and electrolyte flow rates ranged from 0 to 600 $\mu l\,min^{-1}$.

Vanadium redox in acidic media served as our fuel and oxidant. Although vanadium has a lower energy density than methanol or formic acid, it has high activity on bare carbon, high open circuit potential, and can be regenerated [24]. We prepare 50 mM V^{2+} and VO_2^+ in 1 M sulfuric acid through electrolysis of VO^{2+}. At the fuel cell anode the reaction according to Eq. (1) occurs.

$$V^{2+} \leftrightarrow V^{3+} + e^- \quad (E^\circ = -0.255\,V \text{ vs. SHE}) \tag{1}$$

At the cathode, the reaction according to Eq. (2) occurs [32].

$$VO_2^+ + 2H^+ + e^- \leftrightarrow VO^{2+} + H_2O \quad (E^\circ = 0.991\,V \text{ vs. SHE}) \tag{2}$$

Polarization data is recorded galvanostatically and power and current density numbers are normalized by the top projected electrode area of 0.1 cm^2.

3. Results and discussion

3.1. Fuel cell performance

In this section we describe the variation of the fuel cell performance on the flow rate of the reactants, electrolyte, and the concentration of the separation electrolyte. Fig. 3 presents polarization and power density curves for the counter flow fuel cell operating at 50 and 300 $\mu l\,min^{-1}$. In both cases, the reactant concentrations were 50 mM vanadium in 1 M sulfuric acid, and the separation electrolyte was 2 M sulfuric acid with a flow rate of 30 $\mu l\,min^{-1}$. The polarization data shows general fuel cell behavior present in both membraneless [30] and membrane based [33] designs. An initial drop in voltage is due to activation losses at the electrocatalyst surface. The activation decay is followed by a linear region of potential drop due to Ohmic losses in the electrodes and ionic interface. At higher current densities (and low flow rates) a reaction boundary layer at the electrocatalyst surface prevents fresh vanadium from reacting, inducing a sharp drop in cell potential as observed for the 50 $\mu l\,min^{-1}$ case at current densities in excess of 4 $mA\,cm^{-2}$.

Increasing the reactant flow rate should only reduce the mass transport associated losses in the cell potential. The potential losses (activation and Ohmic) are identical to a current density of less than 4 $mA\,cm^{-2}$. In excess of 4 $mA\,cm^{-2}$, the 50 $\mu l\,min^{-1}$ case exhibits lower potentials than the 300 $\mu l\,min^{-1}$ case, which we attribute to

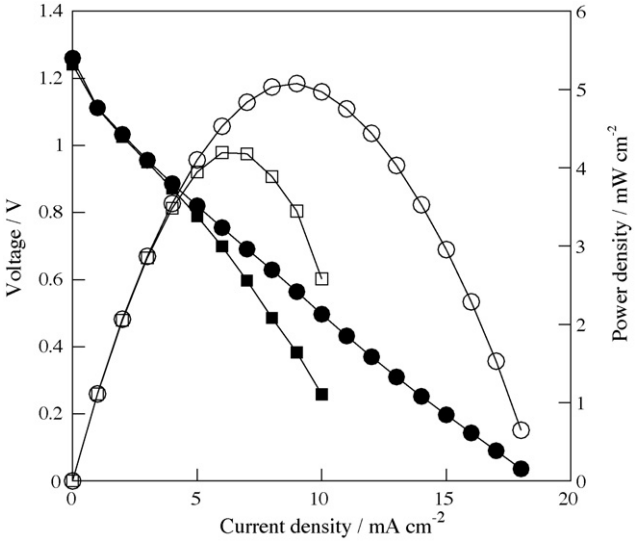

Fig. 3. Polarization (filled symbols) and power density (open symbols) curves for the counter flow fuel cell operating at 50 μl min^{-1} (■) and 300 μl min^{-1} (●), and in both cases the separation electrolyte was at 30 μl min^{-1}. At higher flow rates, reaction and diffusion boundary layers at the electrode surface are thinner, which enhances reactant transport and yields higher currents.

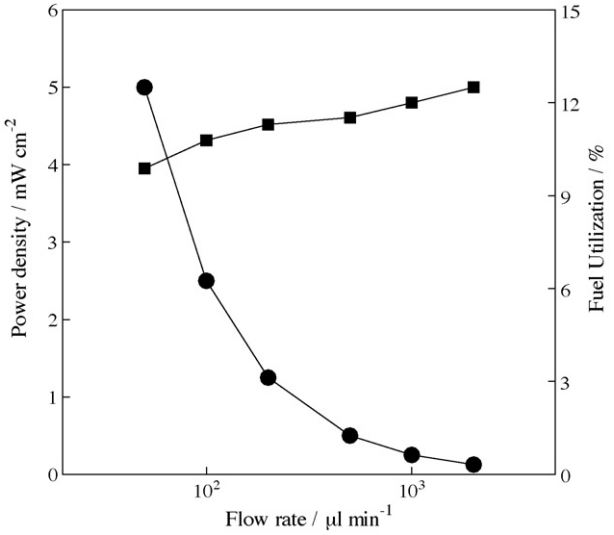

Fig. 5. Power density (■) and fuel utilization (●) as a function of the reactant flow rate, under 5 mA cm^{-2} current density load. The separating electrolyte was fixed at 30 μl min^{-1} and 2 M. There is a drastic decrease in fuel utilization and moderate increase in power density.

mass transport losses at the lower flow rate. We do not observe the drop in potential in the 300 μl min^{-1} case due to an extension of the Ohmic regime. Higher flow rates decrease the thickness of the reaction driven diffusion boundary layers thus enhancing the mass transport of the reactants to the catalyst sites [34].

The counter flow fuel cell features a separation electrolyte that helps maintain physical separation between the fuel and oxidant, while providing a highly conductive ionic interface to complete the electrochemical circuit. Fig. 4 shows the effect of altering the electrolyte flow rate on the fuel cell polarization. The polarization curves show that potential and current density increase by approximately 0.1 V and 3 mA cm^{-2} when the electrolyte flow rate varies from 0 to 600 μl min^{-1}. In a membraneless fuel cell, the electrolyte

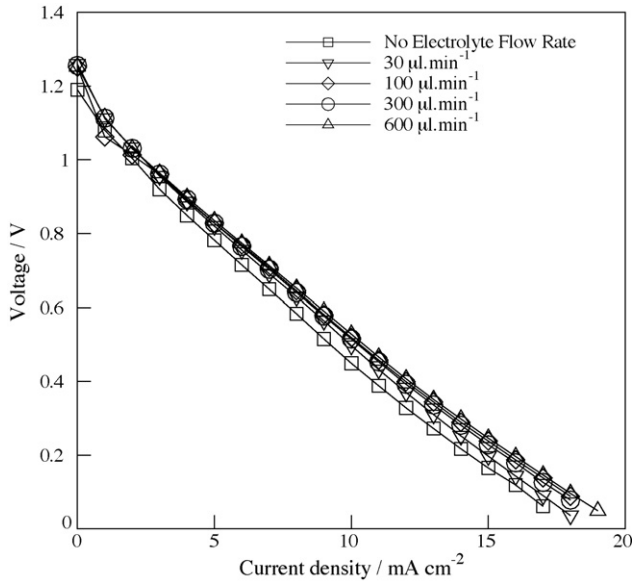

Fig. 4. Fuel cell polarization curves for electrolyte flow rates ranging from 0 to 600 μl min^{-1}. The vanadium reactant concentrations are 50 mM supported in 1 M sulfuric acid flowing at 300 μl min^{-1}. The seperating electrolyte is 2 M sulfuric acid. As the separating electrolyte flow rate increases a marginal increase in overall current density and potential is observed.

provides an electrochemical bridge from the anode to the cathode similar to the role of a semi-permeable membrane in a PEM fuel cell. We expect the resistance to depend on the gap conductivity and geometry. An approximation for the gap's resistance is $R = g/\sigma A$, where g is the gap length between the electrodes, σ is the local conductivity of the solution in the gap, and A is the cross-sectional area of the gap. The separation electrolyte contains a higher concentration of sulfuric acid than the reactant streams and, at higher flow rates, occupies a larger zone in the gap between the electrodes which increases the effective conductivity of the solution. Therefore, the increase in potential is attributed to the reduction in Ohmic losses in the gap. The increase in cell performace is relatively small because the Ohmic losses are largely controlled by the distance between the electrodes, g, which is kept constant throughout our experiments. These results suggest that the minimum electrolyte flow rate may be used to maintain an effective reactant separation.

3.2. Fuel utilization and power density

We have shown that increasing the reactant flow rate increases the fuel cell potential and power. However, the increase in power is at the cost of fuel utilization, described as

$$\eta = \frac{I}{nFCQ}, \tag{3}$$

where I is the measured current at a flow rate Q, n is the number of electrons transferred per mole (1 for vanadium redox), F is Faraday's constant, and C is the concentration of vanadium used (0.05 M). Using Eq. (3) and polarization data from Fig. 3, the maximum fuel utilization at 50 and 300 μl min^{-1} are 24.9 and 8.3%, respectively.

Fig. 5 plots power density and fuel utilization as a function of reactant flow rate. The separation electrolyte was fixed at 30 μl min^{-1} and 2 M, and the sourced current density is 5 mA cm^{-2}. At this current density, the voltage increases from 0.8 to 1.0 V across the flow rate range. As with previous findings [21,22,27], the fuel utilization drops drastically over the flow rate range, while the power increase is not as significant. In our case, a 20% increase in power over the tested flow rates is countered by a 91% drop in fuel utilization.

Eq. (3) suggests that increasing the fuel utilization is best achieved by flowing low concentration reactants at low flow

rates. The reaction residence times, reaction product advection, and transport due to diffusion at the reactant/electrolyte interface are all dependent on the flow rates of the reactants and electrolyte. However, it is also advantageous to expose the reactants to the largest possible electrocatalyst surface. Larger surface areas increase the reaction sites and reduce overall concentration boundary layers, resulting in an increase in extracted current. While the fuel cell can be designed to house larger electrode areas, the counter flow scheme we present allows the reactants to be recycled as they have not mixed.

4. Conclusions

We present a convective counter flow membraneless fuel cell that utilizes vanadium redox species and porous carbon electrocatalyst. The fuel cell architecture allows electrolyte flow rates as low as 30 μl min^{-1} to separate reactants. The reactants remain separated throughout their residence time in the fuel cell, do not mix diffusively, and are collected separately. Increasing the reactant flow rate results in an increase in potential and power density output. However, the increase in power output at higher flow rates results in a drastic loss in fuel utilization.

Acknowledgements

KS acknowledges the Arizona State University Graduate Fellowship Program for financial support. KS also thanks Prof. Erik Kjeang for assistance in preparing the vanadium solutions.

Appendix A. Supplementary data

Supplementary data associated with this article can be found, in the online version, at doi:10.1016/j.jpowsour.2010.03.096.

References

[1] C.K. Dyer, Journal of Power Sources 106 (2002) 31–34.
[2] R. Ferrigno, A.D. Stroock, T.D. Clark, M. Mayer, G.M. Whitesides, Journal of the American Chemical Society 124 (2002) 12930–12931.
[3] J.D. Morse, International Journal of Energy Research 31 (2007) 576–602.
[4] S. Ha, B. Adams, R.I. Masel, Journal of Power Sources 128 (2004) 119–124.
[5] A. Collier, H.J. Wang, X.Z. Yuan, J.J. Zhang, D.P. Wilkinson, International Journal of Hydrogen Energy 31 (2006) 1838–1854.
[6] H. Li, Y.H. Tang, Z.W. Wang, Z. Shi, S.H. Wu, D.T. Song, J.L. Zhang, K. Fatih, J.J. Zhang, H.J. Wang, Z.S. Liu, R. Abouatallah, A. Mazza, Journal of Power Sources 178 (2008) 103–117.
[7] X. Cheng, J.L. Zhang, Y.H. Tang, C.J. Song, J. Shen, D.T. Song, J.J. Zhang, Journal of Power Sources 167 (2007) 25–31.
[8] J.R. Yu, T. Matsuura, Y. Yoshikawa, M.N. Islam, M. Hori, Physical Chemistry Chemical Physics 7 (2005) 373–378.
[9] F.R. Brushett, R.S. Jayashree, W.-P. Zhou, P.J.A. Kenis, Electrochimica Acta 54 (2009) 7099–7105.
[10] F.R. Brushett, W.P. Zhou, R.S. Jayashree, P.J.A. Kenis, Journal of the Electrochemical Society 156 (2009) B565–B571.
[11] S.H. Chan, N.T. Nguyen, Z.T. Xia, Z.G. Wu, Journal of Micromechanics and Microengineering 15 (2005) 231–236.
[12] F.L. Chen, M.H. Chang, M.K. Lin, Electrochimica Acta 52 (2007) 2506–2514.
[13] E.R. Choban, L.J. Markoski, A. Wieckowski, P.J.A. Kenis, Journal of Power Sources 128 (2004) 54–60.
[14] E.R. Choban, P. Waszczuk, P.J.A. Kenis, Electrochemical and Solid State Letters 8 (2005) A348–A352.
[15] J.L. Cohen, D.J. Volpe, D.A. Westly, A. Pechenik, H.D. Abruna, Langmuir 21 (2005) 3544–3550.
[16] J.R. Hayes, A.M. Engstrom, C. Friesen, Journal of Power Sources 183 (2008) 257–259.
[17] R.S. Jayashree, L. Gancs, E.R. Choban, A. Primak, D. Natarajan, L.J. Markoski, P.J.A. Kenis, Journal of the American Chemical Society 127 (2005) 16758–16759.
[18] R.S. Jayashree, M. Mitchell, D. Natarajan, L.J. Markoski, P.J.A. Kenis, Langmuir 23 (2007) 6871–6874.
[19] E. Kjeang, A.G. Brolo, D.A. Harrington, N. Djilali, D. Sinton, Journal of the Electrochemical Society 154 (2007) B1220–B1226.
[20] E. Kjeang, N. Djilali, D. Sinton, T.S. Zhao, Micro Fuel Cells, Academic Press, Boston, 2009, pp. 99–139.
[21] E. Kjeang, J. McKechnie, D. Sinton, N. Djilali, Journal of Power Sources 168 (2007) 379–390.
[22] E. Kjeang, R. Michel, D.A. Harrington, N. Djilali, D. Sinton, Journal of the American Chemical Society 130 (2008) 4000–4006.
[23] E. Kjeang, R. Michel, D.A. Harrington, D. Sinton, N. Djilali, Electrochimica Acta 54 (2008) 698–705.
[24] E. Kjeang, B.T. Proctor, A.G. Brolo, D.A. Harrington, N. Djilali, D. Sinton, Electrochimica Acta 52 (2007) 4942–4946.
[25] S.M. Mitrovski, R.G. Nuzzo, Lab on a Chip 6 (2006) 353–361.
[26] H.B. Park, D.H. Ahmed, K.H. Lee, H.J. Sung, Electrochimica Acta 54 (2009) 4416–4425.
[27] K.S. Salloum, J.R. Hayes, C.A. Friesen, J.D. Posner, Journal of Power Sources 180 (2008) 243–252.
[28] M.H. Sun, G.V. Casquillas, S.S. Guo, J. Shi, H. Ji, Q. Ouyang, Y. Chen, Microelectronic Engineering 84 (2007) 1182–1185.
[29] G.H. Miley, N. Luo, J. Mather, R. Burton, G. Hawkins, L.F. Gu, E. Byrd, R. Gimlin, P.J. Shrestha, G. Benavides, J. Laystrom, D. Carroll, Journal of Power Sources 165 (2007) 509–516.
[30] E. Kjeang, N. Djilali, D. Sinton, Journal of Power Sources 186 (2009) 353–369.
[31] M. Skyllaskazacos, D. Kasherman, D.R. Hong, M. Kazacos, Journal of Power Sources 35 (1991) 399–404.
[32] D.R. Lide (Ed.), CRC Handbook of Chemistry and Physics (Internet Version 2010), 90th ed., CRC Press/Taylor and Francis, Boca Raton, FL.
[33] J. Larminie, A. Dicks, Fuel Cell Systems Explained, 2nd ed., John Wiley & Sons Ltd., 2003.
[34] R.F. Probstein, Physicochemical Hydrodynamics: An Introduction, 2nd ed., Wiley, 2003.